

Supporting Information

Activation of Hydrogen-Evolution Reactivity in an Rh-doped SrTiO₃ Photocatalyst under Visible-Light Irradiation by Loading with Controlled Platinum Nanoclusters

Daichi Yazaki¹, Tokuhiwa Kawawaki^{1,2,*}, Tomoya Tanaka¹, Daisuke Hirayama¹, Yamato Shingyouchi¹, and Yuichi Negishi^{1,2,*}

¹Department of Applied Chemistry, Faculty of Science, Tokyo University of Science, Kagurazaka, Shinjuku-ku, Tokyo 162–8601, Japan

²Research Institute for Science and Technology, Tokyo University of Science, Kagurazaka, Shinjuku-ku, Tokyo 162–8601, Japan

*Corresponding author E-mail: kawawaki@rs.tus.ac.jp (T.K.), negishi@rs.tus.ac.jp (Y.N.)

1 Chemicals

All chemicals were commercially obtained and used without further purification. Hydrogen hexachloroplatinate(VI) hexahydrate (H₂PtCl₆·6H₂O) was obtained from Tanaka Kikinzoku. Sodium hydroxide (NaOH), platinum (Pt) standard solution (1000 mg L⁻¹), bismuth standard solution (100 ppm), boron nitride, barium sulfate, strontium carbonate (SrCO₃), titanium(IV) oxide rutile form (TiO₂), rhodium(III) oxide (Rh₂O₃), iron(II) chloride tetrahydrate (FeCl₂·4H₂O), iron(III) chloride hexahydrate (FeCl₃·6H₂O), vanadium(V) oxide (V₂O₅), bismuth(III) nitrate pentahydrate (Bi(NO₃)₃·5H₂O) and potassium carbonate (K₂CO₃) were obtained from FUJIFILM Wako pure Chemical Co.. Methanol (MeOH), acetone, toluene, ethylene glycol, dichloromethane (DCM), potassium bromide (KBr), tetrahydrofuran (THF) sulfuric acid (H₂SO₄) and nitric acid (HNO₃) were obtained from Kanto Kagaku. 2-Phenylethanethiol was obtained from Sigma Aldrich. *trans*-2-[3-(4-*tert*-Butylphenyl)-2-methyl-2-propenylidene]malononitrile (DCTB), and 4-mercaptobenzoic acid (*p*-MBA) were purchased from Tokyo Kasei. Pure Milli-Q water (>18 MΩ × cm) was generated using a Merck Millipore Direct 3 UV system.

2. Experiments

2.1 Synthesis

Preparation of SrTiO₃:Rh

SrTiO₃:Rh was synthesized based on a previous report.¹ First, SrCO₃ treated in air at 200 °C for 1 h before use (1.581 g), TiO₂ (0.791 g), Rh₂O₃ (19.2 mg) were grinded with a small amount of MeOH and then the mixtures were calcined in air at 900 °C for 1 h using an alumina crucible. Second, the product was grinded and calcined in air at 1100 °C for 10 h using an alumina crucible to obtain the desired SrTiO₃:Rh.

Preparation of BiVO₄

BiVO₄ was synthesized based on a previous report.² First, K₂CO₃ (1.6584 g) and V₂O₅ (3.6376 g) were mixed on a petri dish. The obtained mixtures were calcined in air at 445 °C for 5 h using an alumina crucible. The obtained powder (K₃V₅O₁₄) was used as a precursor of BiVO₄. Next, water (50 mL) and HNO₃ (1.85 mL) were added to an Erlenmeyer flask. To the mixture, Bi(NO₃)₃·5H₂O (4.8507 g) and K₃V₅O₁₄ (1.1920

g) were added and stirred under dark for 3 days. The yellow powder was collected by centrifugation and washed with water until the pH became 7. Finally, the powder was calcined in air at 495 °C for 10 h using an alumina crucible to obtain the desired powder.

Synthesis of Pt₋₅₁(PET)_n(CO)_m(*p*-MBA)_l

Pt₋₅₁(PET)_n(CO)_m was synthesized by polyol reduction and ligand exchange. First, 135 mg of NaOH was dissolved in 15 mL of ethylene glycol, and then 104 mg of hexachloroplatinic acid (H₂PtCl₆) was dissolved in the solution. The solution was heated at 80 °C for 15 min. The Pt ions were then reduced by heating the solution at 120 °C for 30 min. After the solution was cooled to 25 °C, PET was added to exchange the ligands of the Pt NCs. Finally, the ligand (PET, CO)-protected Pt NCs (Pt₋₅₁(PET)_m(CO)_l) were purified by washing with ultrapure water and MeOH. Then, 3 mg of Pt₋₅₁(PET)_m(CO)_l was dissolved in 1 mL of THF. To this solution was added 3 mg of *p*-MBA, and the solution was left to sit at room temperature for 2 h. The obtained product was evaporated to dryness, and then the dried product was washed with a mixture of MeOH and water (1:9) to remove excess thiol and other byproducts. This operation was repeated three times. The obtained Pt₋₅₁(PET)_n(CO)_m(*p*-MBA)_l was then reacted again with *p*-MBA under the same experimental conditions to increase the number of *p*-MBA ligands. The product was washed with a mixture of MeOH and water (1:9), and pure Pt₋₅₁(PET)_n(CO)_m(*p*-MBA)_l was isolated from the dried product with THF.

Preparation of Pt_{NC}/STO:Rh

STO:Rh (200 mg) and THF (10 mL) were added to a vial and dispersed by ultrasonication for 15 min. THF solution containing the objective loading amount of Pt₋₅₁(PET)_n(CO)_m(*p*-MBA)_l was added with vigorous stirring to obtain a total volume of 20 mL. After 3 h, the powder was collected by centrifugation and dried under reduced pressure. To determine the actual adsorbed amount of Pt₋₅₁(PET)_n(CO)_m(*p*-MBA)_l, the amount of Pt contained in the supernatant solution was measured by inductively coupled plasma mass spectrometry (ICP-MS). The obtained powder was placed in an electric oven, the temperature was increased to 300 °C at 7 °C min⁻¹ under reduced pressure, and heating was continued for 80 min to obtain Pt_{NC}/STO:Rh.

Preparation of Pt_{PD}/STO:Rh

Pt_{PD}/STO:Rh loaded with Pt nanoparticles (NPs) by the photodeposition (PD) method was prepared based on a previous report.³ STO:Rh (200 mg) and ultrapure water (108 mL) were added to a top-irradiation reaction vessel and dispersed by ultrasonication for 15 min. While stirring the obtained suspension, the objective loading amount of H₂PtCl₆ and 12 mL of MeOH were added. After replacing the air in the solution with argon (Ar), the Ar flow rate was adjusted to 12 mL min⁻¹ and the solution was irradiated with a Xenon (Xe) lamp (PerkinElmer, Cermax PE300BF) for 2 h. The powder was collected by centrifugation and dried to obtain Pt_{PD}/STO:Rh.

2.2 Characterization

The diffuse reflection (DR) spectra were acquired at ambient temperature with a V-670 spectrometer (JASCO, Tokyo, Japan). The wavelength-dependent optical data [$I(w)$] were converted to energy-dependent data [$I(E)$] with the following equation that conserved the integrated spectral areas: $I(E) = I(w)/|\partial E/\partial w| \propto I(w) \times w^2$.

The powder X-ray diffraction (PXRD) patterns of the samples were measured with a Rint2500 diffractometer (Rigaku) using Cu-K α source operated at 40 kV and 200 mA. A reflection-free silicon plate was used as a substrate.

The transmission electron microscope (TEM) images were recorded with a H-9500 electron microscope (HITACHI, Tokyo, Japan) or JEM-2100 electron microscope (JEOL, Tokyo, Japan) operating at 200 kV, typically using magnification of 600,000.

Pt L₃-edge X-ray absorption fine structure (XAFS) measurements were performed at beamline BL01B1 of the SPring-8 facility of the Japan Synchrotron Radiation Research Institute (proposal numbers: 2021A1102, 2021B1163, 2022A1075 and 2022B1823). The incident X-ray beam was monochromatized by a Si(111) double-crystal monochromator. As references, XAFS spectra of Pt foil and PtO₂ powder were recorded in transmission mode using ionization chambers. The Pt L₃-edge XAFS spectra of the samples were measured in fluorescence mode using a 19-element Ge solid-state detector at 25 °C. The X-ray energies for the Pt L₃-edges were calibrated using Pt foil. The X-ray absorption near edge structure (XANES) and extended X-ray absorption fine structure (EXAFS) spectra were analyzed using xTunes⁴ as follows. The χ spectra were extracted by subtracting the atomic absorption background using cubic spline interpolation and normalized to the edge height. The normalized data were used as the XANES spectra. The k^3 -weighted χ spectra in the k range 3.0–14.0 Å⁻¹ for the Pt L₃-edge were Fourier transformed into r space for structural analysis.

The and sulfur (S) 2p X-ray photoelectron spectroscopy (XPS) spectra were collected by using a JPS-9010MC electron spectrometer (JEOL, Tokyo, Japan) at a base pressure of $\sim 2 \times 10^{-8}$ Torr. X-rays from the Mg-K α line (1253.6 eV) were used for excitation. Each NCs was deposited on an Ag plate and the spectra were calibrated with the peak energies of Ag 3d_{5/2} (368.22 eV).

The ultraviolet-visible (UV-Vis) absorption spectra of products were acquired in THF solution at room temperature with a V-670 spectrometer (JASCO, Tokyo, Japan).

Fourier transform infrared (FT-IR) spectra of the product were obtained using the attenuated total reflectance (ATR) method in the region between 400 and 4000 cm⁻¹ by a FT/IR-4600 spectrometer (JASCO, Tokyo, Japan) equipped with a DLATGS detector as the average of 50 scans at 4 cm⁻¹ resolution.

The matrix-assisted laser desorption/ionization (MALDI) mass spectra were recorded with a JMS-S3000 spiral time-of-flight mass spectrometer (JEOL, Tokyo, Japan) equipped with a semiconductor laser ($\lambda = 349$ nm). DCTB was used as the MALDI matrix. To minimize NC dissociation induced by laser irradiation, the NC-to-matrix ratio was fixed at 1:1000.

ICP-MS was performed with an Agilent 7850c spectrometer (Agilent Technologies, Tokyo, Japan). Bismuth was used as the internal standard. The ICP-MS measurements were performed for the supernatant obtained after mixing Pt NC with the photocatalyst to estimate the unadsorbed or loaded Pt content.

N₂ adsorption was measured at -196 °C on a BELSORP-mini II (BEL Japan Inc., Japan) after preheating under vacuum at 200 °C for 12 h. Specific surface area was estimated by Brunauer-Emmett-Teller (BET) equation with the 0.05–0.25 relative pressure range.

2.3 Photocatalytic measurements

Measurements of photocatalytic hydrogen evolution activity

The photocatalytic hydrogen evolution reaction was carried out at 25 °C using a flow system with a top-irradiation reaction cell. The reaction was performed with an Ar gas flow rate of 12 mL min⁻¹. Photocatalyst powder (0.1 g) was dispersed in an aqueous solution (120 mL) containing 10 vol% MeOH as a hole scavenger. The suspension was irradiated with visible light using a 300 W Xe lamp (PerkinElmer, Cemax PE300BF) with a long-pass filter (HOYA L42). The amounts of evolved gases were determined using an online gas chromatograph (Shimadzu, GC-8A, MS-5A column, TCD, Ar carrier).

Measurements of water-splitting activity

The photocatalytic water-splitting reaction was carried out at 25 °C using a flow system with a top-irradiation reaction cell. The reaction was performed with an Ar gas flow rate of 12 mL min⁻¹. Powders of Pt-cocatalyst loaded SrTiO₃:Rh (0.1 g) and BiVO₄ (0.1 g) were dispersed in an aqueous solution (120 mL) containing Fe ion (FeCl₂ or FeCl₃) as an electron mediator. H₂SO₄ was used as a pH adjuster (pH: 2.4). The suspension was irradiated with visible light using a 300 W Xe lamp (PerkinElmer, Cemax PE300BF) with a long-pass filter (HOYA L42). The amounts of evolved gases were determined using an online gas

chromatograph (Shimadzu, GC-8A, MS-5A column, TCD, Ar carrier).

2.4 Estimation of surface atoms of Pt cocatalysts

Ratio of active site was calculated from arbitrarily assumed face-centered cubic (FCC) structured Pt and diameter of Pt cocatalyst. From the Pt particle model from the FCC structure, the ratio of the number of surface atoms to the total number of atoms was calculated for each atomic layer, and exponential fitting was performed. Furthermore, the estimated total number of atoms was calculated from the correlation between the particle size obtained from the TEM images and the Pt–Pt bond distance (0.256 nm). From the obtained total number of atoms, the ratio of the number of surface atoms was calculated.

3. Table

Table S1. BET specific surface area of STO:Rh and Pt cocatalyst-loaded STO:Rh

Sample	BET specific surface area / $\text{m}^2 \text{g}^{-1}$
STO:Rh	2.5
$\text{Pt}_{-51}(\text{PET})_n(\text{CO})_m(p\text{-MBA})_l/\text{STO:Rh}$	2.9
$\text{Pt}_{\text{NC}}/\text{STO:Rh}$	2.7

Table S2 Possible assignments of peaks observed in FT-IR spectrum of $\text{Pt}_{-51}(\text{PET})_n(\text{CO})_m(p\text{-MBA})_l$

Wavenumber / cm^{-1}	Assignment ^a
2958.3	$\delta(\text{C}-\text{C})$ ethyl
2871.5	$\delta(\text{C}-\text{H})$ methyl
2562.9	$\delta(\text{S}-\text{H})$
1681.6	$\delta(\text{C}=\text{O})$
1594.8	$\delta(\text{C}=\text{C})$ phenyl
1427.1	$\nu(\text{O}-\text{H}\cdots\text{O})$ or $\delta(\text{C}-\text{OH})$
1326.8	$\nu(\text{O}-\text{H}\cdots\text{O})$ or $\delta(\text{C}-\text{OH})$
1182.2	$\nu(\text{C}-\text{H})$ phenyl
1097.3	$\nu(\text{C}-\text{H})$ phenyl
927.6	$\nu(\text{O}-\text{H})$
848.5	$\nu(\text{C}-\text{H})$ phenyl
757.9	$\delta(\text{C}-\text{H})$ phenyl

^a See Reference.⁵⁻⁷

Table S3 Results of solubility test for before and after ligand exchange reaction of Pt NC.

Sample	Water	Acetone	MeOH	THF	DCM
$\text{Pt}_{-51}(\text{PET})_n(\text{CO})_m$	Insoluble	Insoluble	Insoluble	Soluble	Soluble
$\text{Pt}_{-51}(\text{PET})_n(\text{CO})_m(p\text{-MBA})_l$	Insoluble	Soluble	Soluble	Soluble	Soluble

Table S4. H_2 -evolution activity of Pt cocatalyst-loaded $\text{SrTiO}_3:\text{Rh}$

Sample	Loading weight of Pt cocatalyst / wt%	HER activity ^a / $\mu\text{mol h}^{-1}$	Diameter of Pt cocatalyst / nm	Ratio of active site ^b	HER activity per active site ^c / $10^{-27} \text{mol s}^{-1} \text{atom}_{\text{Pt}}^{-1}$
$\text{Pt}_{\text{NC}}/\text{STO:Rh}$	0.4	24.7	1.5	0.63	8.87
$\text{Pt}_{\text{PD}}/\text{STO:Rh}$	0.4	19.1	2.8	0.40	10.8

^aActivity of H_2 -evolution reaction (HER rate) was measured by using a long-pass ($>410 \text{ nm}$) filter. ^b Ratio of active site was calculated from section 2.4 in Supporting Information. ^c HER activity per active site was calculated from by dividing moles of H_2 molecules evolved by active sites which are normalized by the amount of Pt active site (HER activity per active site = HER activity/(Loading weight of Pt cocatalyst \times Ratio of active site)).

4. Additional Figures

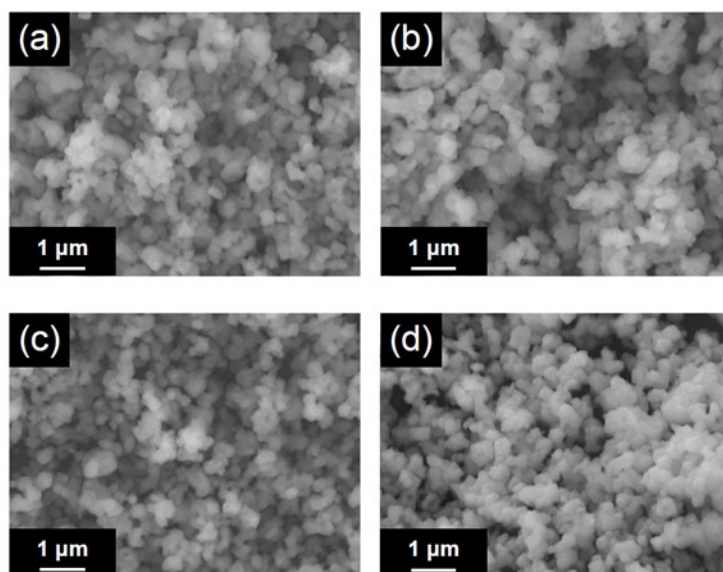


Fig. S1 SEM images of STO:Rh (a) after synthesis (STO:Rh), (b) after Pt NC adsorption ($\text{Pt}_{-51}(\text{PET})_n(\text{CO})_m(p\text{-MBA})_l/\text{STO:Rh}$), (c) after calcination ($\text{Pt}_{\text{NC}}/\text{STO:Rh}$) and (d) after light irradiation ($\text{Pt}_{\text{NC}}/\text{STO:Rh}$ -light).

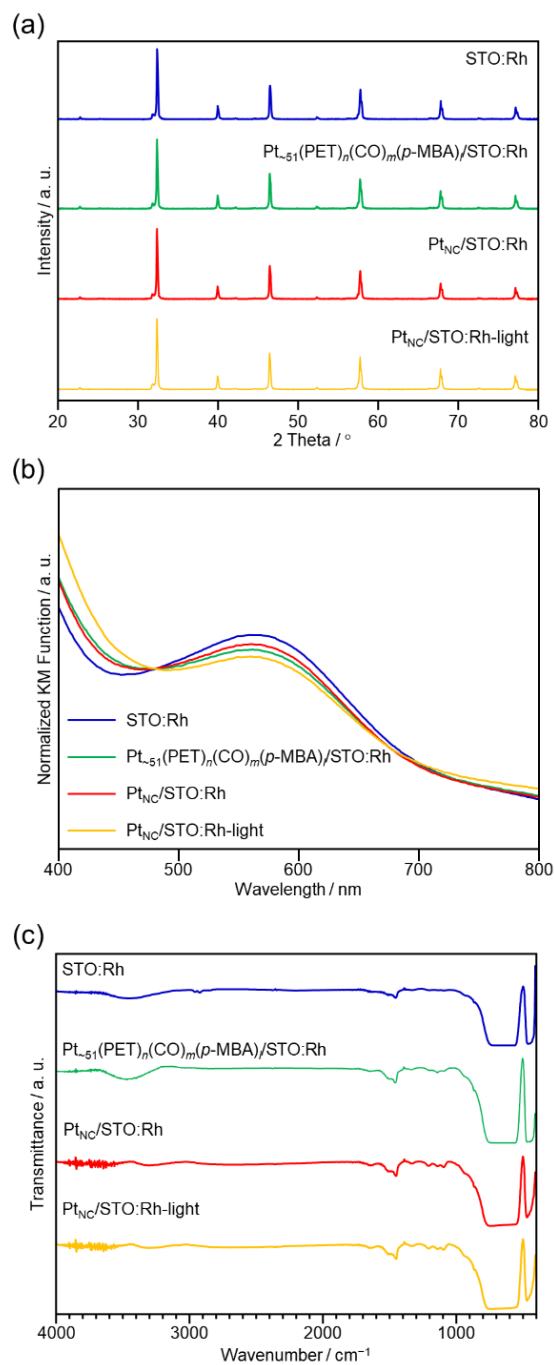


Fig. S2 (a) PXRD patterns, (b) DR spectra and (c) FT-IR spectra of STO:Rh, Pt₋₅₁(PET)_n(CO)_m(*p*-MBA)/STO:Rh, Pt_{NiC}/STO:Rh and Pt_{NiC}/STO:Rh-light.

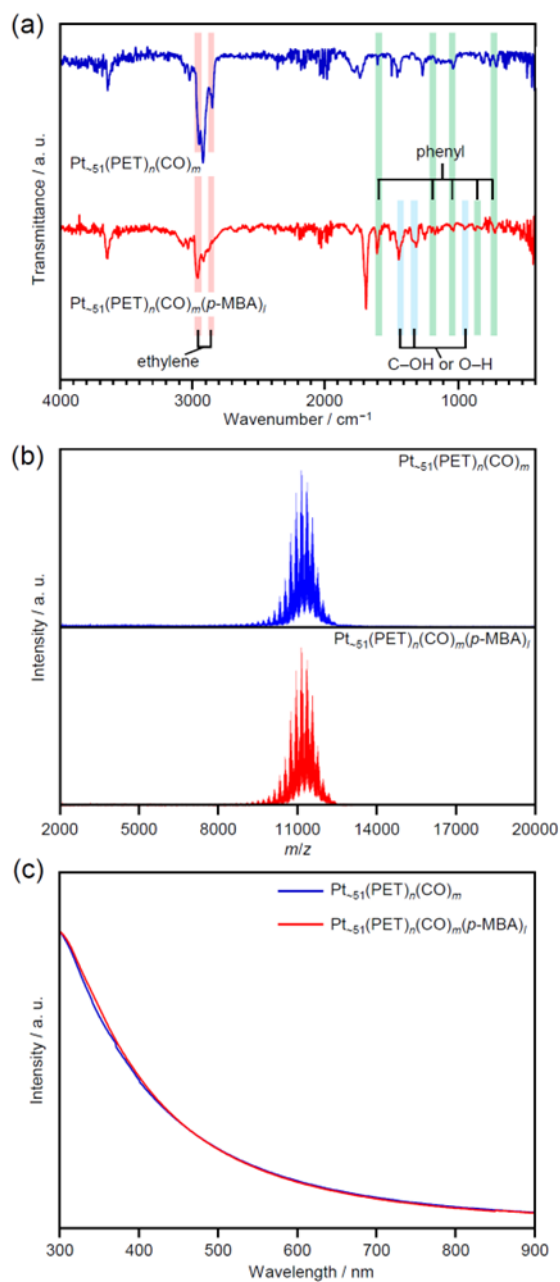


Fig. S3 Results of (a) FT-IR, (b) MALDI-MS, (c) UV-Vis absorption of synthesized Pt NC before ($\text{Pt}_{-51}(\text{PET})_n(\text{CO})_m$) and after ($\text{Pt}_{-51}(\text{PET})_n(\text{CO})_m(p\text{-MBA})_i$) ligand exchange reaction. In (b), both spectra showed a similar mass distribution regardless Pt NC with the different ligands (*i.e.*, PET and *p*-MBA), thus supporting the interpretation that S-C dissociation also occurred before and after ligand exchange.⁷

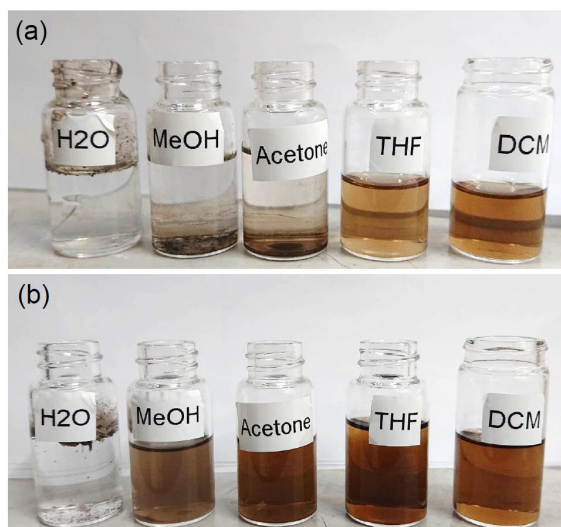


Fig. S4 Photographs for (a) $\text{Pt}_{-51}(\text{PET})_n(\text{CO})_m$ and (b) $\text{Pt}_{-51}(\text{PET})_n(\text{CO})_m(p\text{-MBA})_l$ dissolved in the solutions with different polarity. After ligands exchange, solubility of Pt NC in the solutions with high polarity was improved.

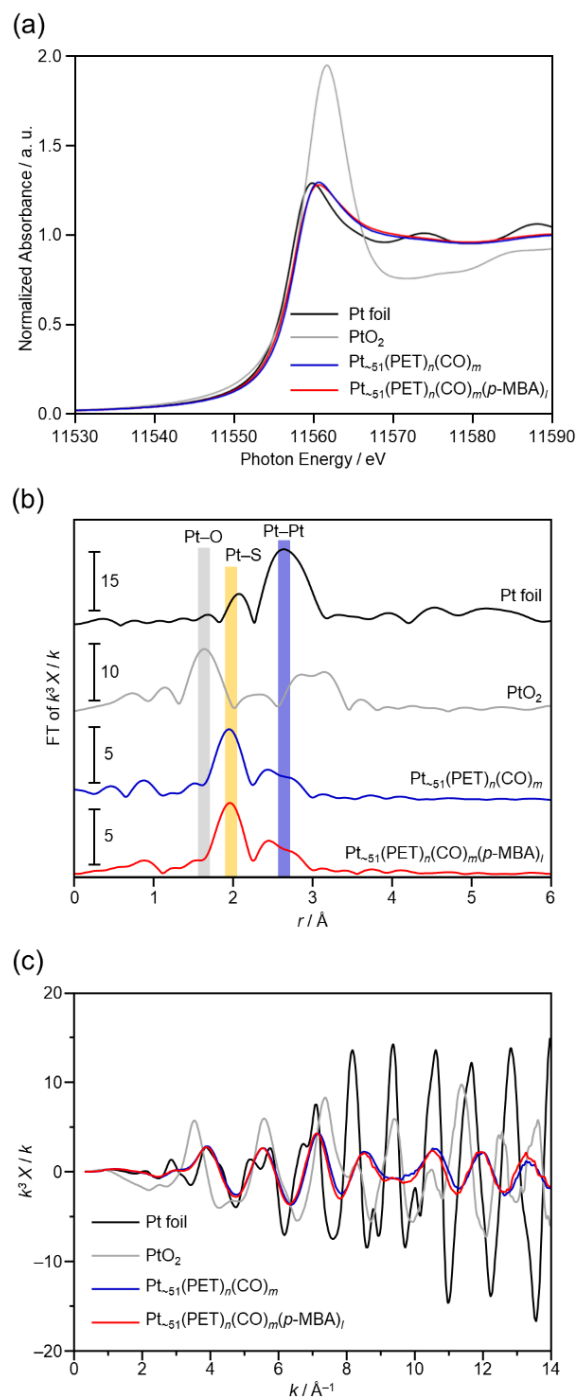


Fig. S5 Results of Pt L₃-edge (a) XANES, (b) FT-EXAFS and (c) EXAFS spectra for Pt-₅₁(PET)_{*n*}(CO)_{*m*} and Pt-₅₁(PET)_{*n*}(CO)_{*m*}(*p*-MBA)_{*l*}, together with Pt foil and PtO₂. In (b), the peaks at ~1.8, ~2.0 and 2.2–3.0 Å are assigned to the Pt–O(C), Pt–S and Pt–Pt bond, respectively.⁸

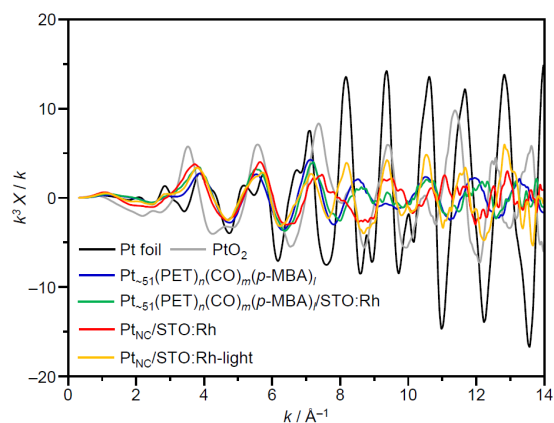


Fig. S6 Results of Pt L₃-edge EXAFS spectra for Pt₋₅₁(PET)_n(CO)_m(p-MBA)_l, Pt₋₅₁(PET)_n(CO)_m(p-MBA)/STO:Rh, Pt_{NC}/STO:Rh and Pt_{NC}/STO:Rh-light. together with Pt foil and PtO₂.

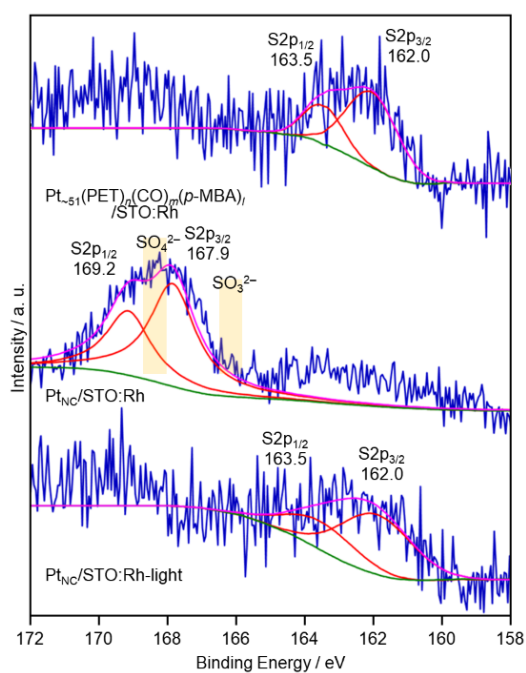


Fig. S7 Results of S 2p XPS spectra for Pt₋₅₁(PET)_n(CO)_m(p-MBA)_l/STO:Rh, Pt_{NC}/STO:Rh and Pt_{NC}/STO:Rh-light.

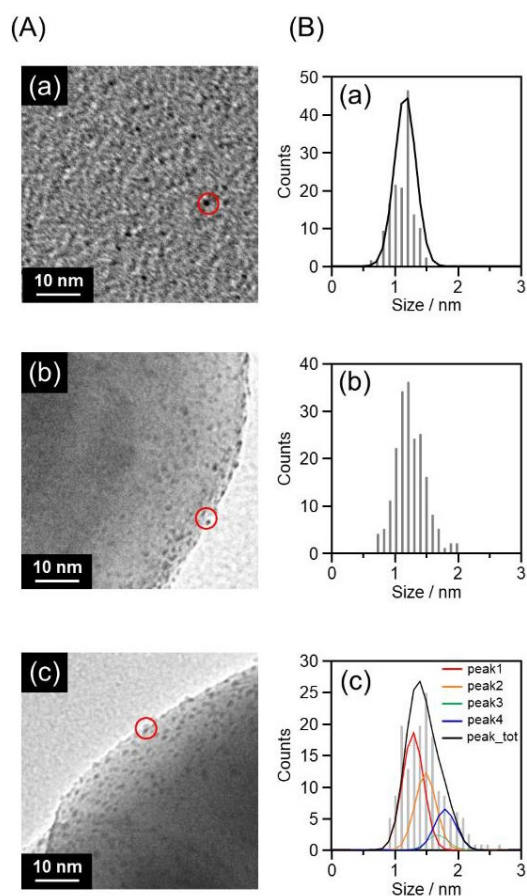


Fig. S8 (A) TEM images and (B) resulting histograms for particle-size distribution of (a) $\text{Pt}_{-51}(\text{PET})_n(\text{CO})_m(p\text{-MBA})_l$, (b) $\text{Pt}_{-51}(\text{PET})_n(\text{CO})_m(p\text{-MBA})_l/\text{STO}:\text{Rh}$ and (c) $\text{Pt}_{\text{NC}}/\text{STO}:\text{Rh}$. It was observed the Pt NCs with an average diameter were 1.2 ± 0.2 nm, 1.3 ± 0.2 nm and 1.5 ± 0.3 nm for $\text{Pt}_{-51}(\text{PET})_n(\text{CO})_m(p\text{-MBA})_l$, $\text{Pt}_{-51}(\text{PET})_n(\text{CO})_m(p\text{-MBA})_l/\text{STO}:\text{Rh}$ and $\text{Pt}_{\text{NC}}/\text{STO}:\text{Rh}$, respectively. The histograms for particle-size distribution of Pt cocatalysts for $\text{Pt}_{\text{NC}}/\text{STO}:\text{Rh}$ were fitted by presumed diameter of Pt_{51} with five- (peak1; 1.29 nm), four- (peak2; 1.49 nm), three- (peak3; 1.68 nm) and two- (peak4; 1.80 nm) layered structure of it from Fig. S9 by Gaussian function. Thus, it was presumed that 92.8% of Pt_{NC} on $\text{Pt}_{\text{NC}}/\text{STO}:\text{Rh}$ have three-dimensional structures (Fig. S9a and b) rather than flat shapes (Fig. S9c and d) of Pt_{-51} .

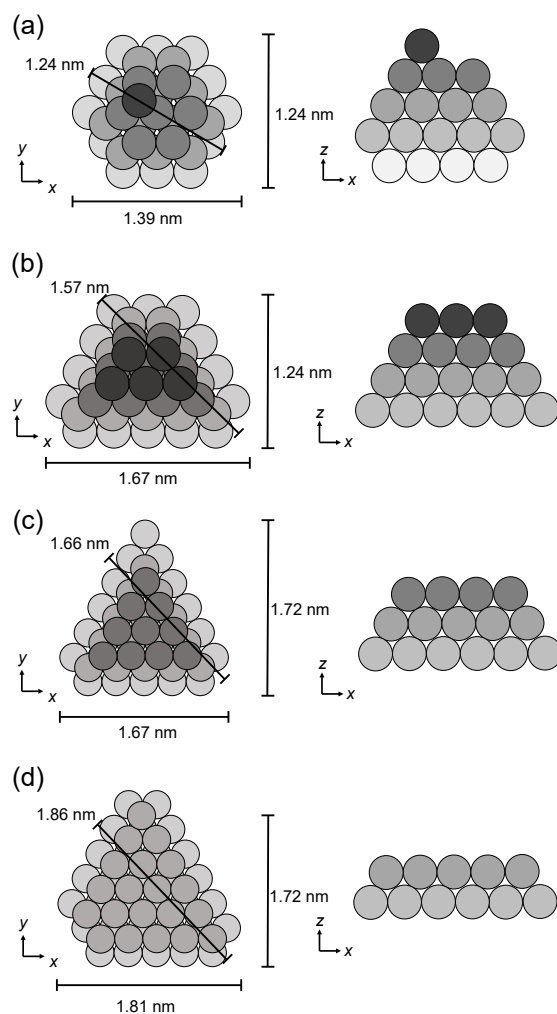


Fig. S9 Possible structures of (a) five, (b) four, (c) three and (d) two-layered Pt₅₁ on STO:Rh. From the size of Pt NCs ($1.5 \text{ nm} \pm 0.3 \text{ nm}$) on STO:Rh obtained by TEM images of Pt_{NC}/STO:Rh (Fig. 3a), it was presumed that Pt NCs have these several-layered structures on STO:Rh (Fig. S8). The sizes of Pt NCs were estimated using Pt–Pt bond length of bulk Pt.

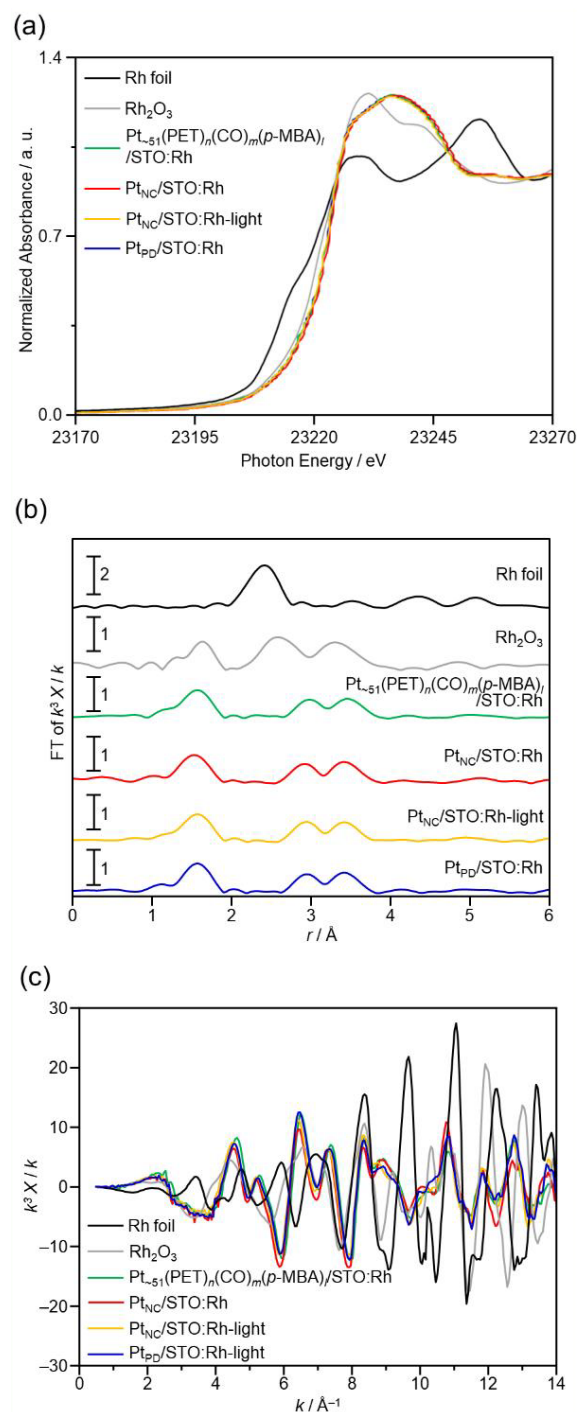


Fig. S10 Rh K-edge (a) XANES, (b) FT-EXAFS and (c) EXAFS spectra of Pt₋₅₁(PET)_n(CO)_m(p-MBA)_i/STO:Rh, Pt_{nC}/STO:Rh, Pt_{nC}/STO:Rh-light and Pt_{pD}/STO:Rh. Rh foil and Rh₂O₃ are also shown for comparison. The electronic state of Pt_{nC}/STO:Rh-light was confirmed that no significant changes compare with before light irradiation (Pt_{nC}/STO:Rh) because STO:Rh-light itself was oxidized by air before the measurement.

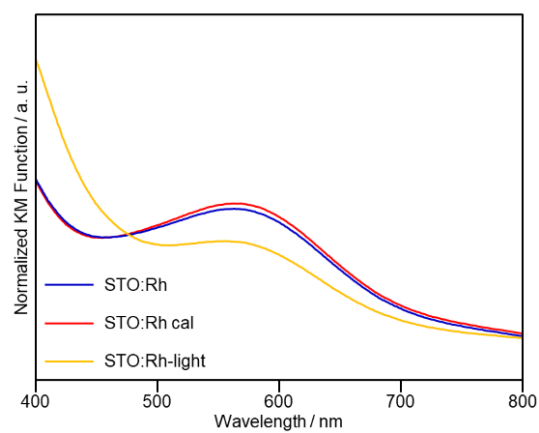


Fig. S11 DR spectra of STO:Rh and after calcination at 300 °C for STO:Rh (STO:Rh cal) and after light irradiation of STO:Rh cal (STO:Rh-light), without Pt cocatalysts. After calcination at 300 °C under reduced pressure, Rh⁴⁺ charge state of STO:Rh was slightly increased. After photoirradiation, Rh⁴⁺ charge state of STO:Rh was largely reduced to Rh³⁺ charge state.

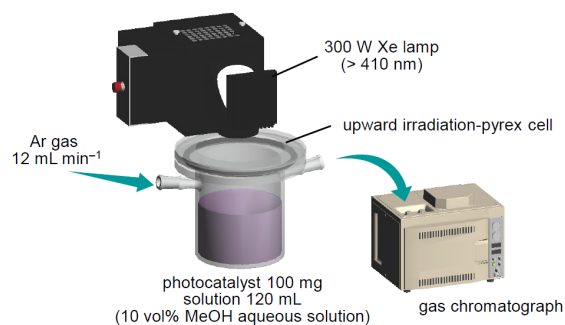


Fig. S12 Schematic illustration of the experimental setup of photocatalytic activity test.

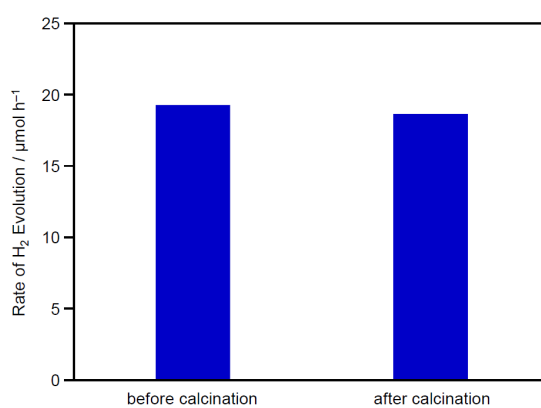


Fig. S13 H₂-evolution activity for Pt_{pD}/STO:Rh using STO:Rh before and after calcination at 300 °C.

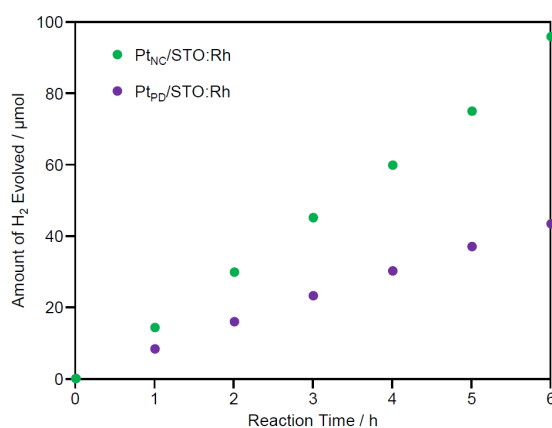


Fig. S14 Time course of H₂-evolution activity for Pt_{nC}/STO:Rh and Pt_{pD}/STO:Rh. The differences in the activity of Pt_{nC}/STO:Rh and Pt_{pD}/STO:Rh compare with Fig. 5c are originated from the difference in the activity of each synthesized batch of STO:Rh in the experiments.

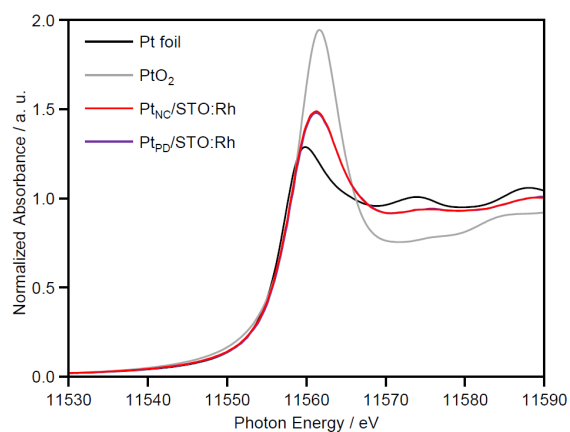


Fig. S15 Results of Pt L₃-edge XANES spectra for Pt_{NC}/STO:Rh and Pt_{PD}/STO:Rh after light irradiation, together with Pt foil and PtO₂.

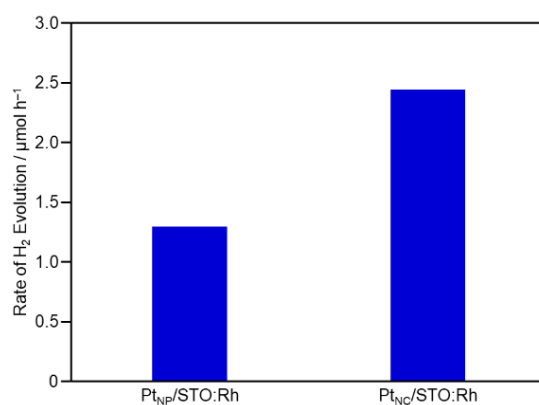


Fig. S16 H₂-evolution activity for Pt_{NC}/STO:Rh and Pt_{PD}/STO:Rh in water with 2 mmol L⁻¹ FeCl₂ as a sacrificial agent. Light source: a 300 W Xe lamp with a long-pass filter (>410 nm), catalyst: 100 mg for each catalyst, reactant solution: 120 mL of 2 mmol L⁻¹ FeCl₂ in H₂SO₄ aq. (pH: 2.4).

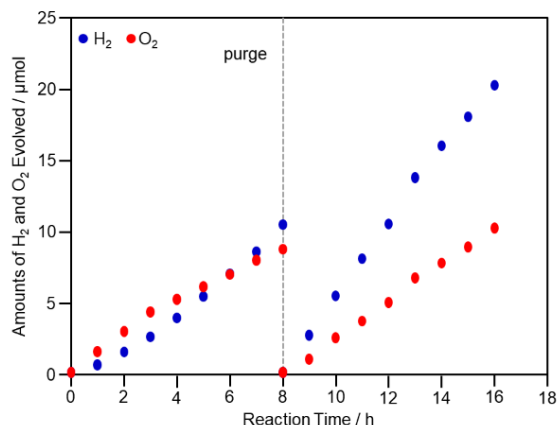


Fig. S17 Time course of water-splitting activity over the Pt_{NC}/STO:Rh-BiVO₄ composite Z-scheme system using FeCl₃ as mediator.

light source: a 300 W Xe lamp with a long-pass filter (>410 nm), Catalyst: 100 mg for each catalyst, reactant solution: 120 mL of 2 mmol L⁻¹ FeCl₃ in H₂SO₄ aq. (pH: 2.4), reaction cell: a top-window reaction cell.

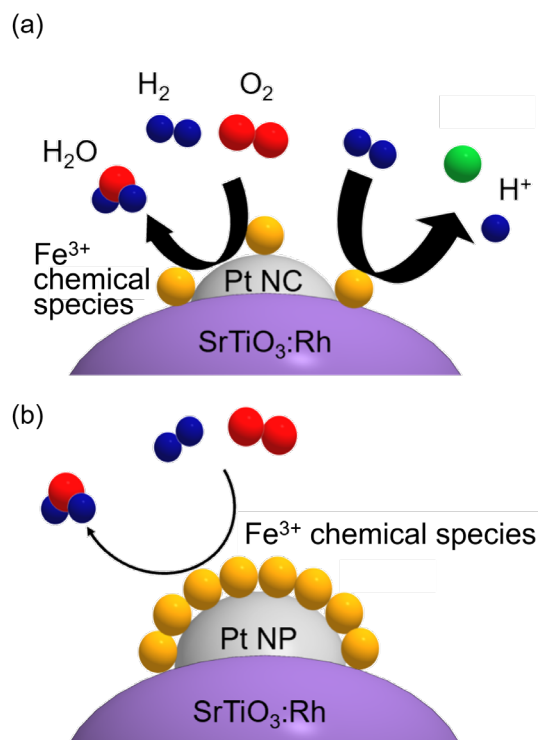


Fig. S18 Schematic of the mechanism of Z-scheme system for (a) Pt_{NC}/STO:Rh and (b) Pt_{NP}/STO:Rh using FeCl₃ as mediator. It was reported that Fe³⁺ chemical species generated by excess Fe³⁺ can be adsorbed on the surface of Pt cocatalyst to suppress reverse reactions.⁹ However, it is considered that the amount of H₂ production was limited because such a protecting effect was difficult to occur on Pt NC.

5. Reference

- 1 R. Konta, T. Ishii, H. Kato and A. Kudo, *J. Phys. Chem. B*, 2004, **108**, 8992–8995.
- 2 A. Kudo, K. Omori, and H. Kato, *J. Am. Chem. Soc.*, 1999, **121**, 11459–11467.
- 3 M. Antuch, P. Millet, A. Iwase, and A. Kudo, *Electrochim. Acta*, 2019, **297**, 696–704.
- 4 H. Asakura, S. Yamazoe, T. Misumi, A. Fujita, T. Tsukuda and T. Tanaka, *Radiat. Phys. Chem.*, 2020, **175**, 108270.
- 5 H. M. Badawi, *Spectrochim. Acta, Part A*, 2011, **82**, 63–68.
- 6 S. E. Creager and C. M. Steiger, *Langmuir*, 1995, **11**, 1852–1854.
- 7 T. Kawawaki, N. Shimizu, K. Funai, Y. Mitomi, S. Hossain, S. Kikkawa, D. J. Osborn, S. Yamazoe, G. F. Metha and Y. Negishi, *Nanoscale*, 2021, **13**, 14679–14687.
- 8 T. Imaoka, Y. Akanuma, N. Haruta, S. Tsuchiya, K. Ishihara, T. Okayasu, W.-J. Chun, M. Takahashi and K. Yamamoto, *Nat. Commun.*, 2017, **8**, 688.
- 9 H. Kato, Y. Sasaki, A. Iwase and A. Kudo, *Bull. Chem. Soc. Jpn.*, 2007, **80**, 2457–2464.